LANDSLIDE INVENTORY MAPPING USING AIRSAR DATA AND OPTICAL SATELLITE IMAGES IN CAMERON HIGHLANDS AREA, MALAYSIA

[1]HIMAN SHAHABI, [2]BAHARIN BIN AHMAD

[1]Department of Geomorphology, Faculty of Natural Resources, University of Kurdistan, Sanandaj, Iran 2 Department of Geoinformation, Faculty of Geoinformation and Real Estate, Universiti Teknologi Malaysia (UTM), Malaysia
E-mail: [1]h.shahabi@uok.ac.ir, [2]baharinahmad@utm.my

Abstract - Landslide hazard is more critical for human settlement at hill sites, particularly in tropical countries like Malaysia where heavy precipitation can causes landslides. In the landslide inventory map including all 92 landslide locations was created based on numerous resources such as digital aerial photographs, AIRSAR data, WorldView-1, SPOT 5 satellite images, and field surveys. The results indicated the accuracy of SAR data and optical satellite images using the root mean square error (RMSE) method was 0.163, which indicate acceptable agreement relating to landslide points detected and the current data from landslide areas.

Key Words - Landslide detection; SAR data; optical satellite images; Malaysia.

I. INTRODUCTION

Natural disasters such as hurricanes, earthquakes, erosion, tsunamis, and landslides cause the loss of human life and damage to property, and of these landslide can be accepted as one of most important natural disasters worldwide [48]. Statistics from the Center for Research on the Epidemiology of Disasters (CRED) show that landslides are responsible for at least 17% of all natural hazard fatalities worldwide [32]. Landslide hazard assessment and risk reduction can be accomplished by providing risk managers with easily accessible, continuous, and accurate information about landslide occurrence. Thus, an accurate susceptibility mapping can be key information for a large variety of users from both private and public sectors, from governmental departments and the scientific community and from local to international levels [8]. In Cameron highlands area in Malaysia, landslide mapping is difficult since the landslides are generally covered by dense vegetation and the cloudy and rainy weather conditions are often undesirable for optical remote sensing data [38]. Consequently, the use of new techniques and accurate data to landslide susceptibility mapping in the tropical environment is a necessity. The lack of reliable landslide inventory maps prevents the assessment of landslide hazard and risk, which may subsequently complicate the implementation of mitigation measures.

In recent years, radar has given a new dimension to disaster management research by providing real-time and precise information [14]. Synthetic aperture radar (SAR) is an active remote sensing system which has the capability of data collection day and night under all weather conditions. In recent years, SAR data are increasingly applied to natural hazards' researches, either by themselves or in combination with data from other remote sensing sensors [13]. SAR data such as amplitude and SAR polarimetric (POLSAR) images, interferometric DEM and other products of the interferometric DEM have proven useful [31]. The combination of both optical and SAR data can also be utilized in geo-hazards identification and mapping to complement analysis. The SAR technique is highly popular in landslide studies [7].

Thus, remote sensing can play a role in the production of a landslide inventory map and in the generation of thematic maps related to landslide occurrences. Several previous works have showed the potential of remote-sensing data both in the extraction of causal factors which are linked to landslide occurrences and finding landslide areas 15, 28]. The main objective of this study is to assess the potential of AIRSAR data together with C-, L- and P-band images and WorldView-1 images for producing landslide inventory maps in the tropical forest namely in the Cameron Highlands, Malaysia.

II. DESCRIPTION OF STUDY AREA

The Research Site is part of Cameron Highlands bounded by Longitudes 101˚ 20' 21''E to 101˚ 26' 50''E and Latitudes 4˚ 24' 37'' N to 4˚ 33' 19'' N (Geographic Lat/Lon WGS 84 Projection) [34]. The research area encompasses an area of 38.4 km2 and is situated near the northern central part of Peninsular Malaysia in Pahang state which is one of the 13 states of Malaysia (Fig. 1). The geomorphology of the area is rough and has altitude ranging from 840 m to 2110 m. It has an estimated 15% flat terrain situated adjacent and extending to the main river. The hilly areas

dominate the western and north western parts, in which Mt. Irau is the highest peak at 2110 m. Bertam and Telom Rivers are the main drainage features in this area. Its valley and tributaries are mainly flowing from north-northwest to south-southeast [35]. Megacrystic biotite granites are the most common geological structure of central mountain chain in Peninsular Malaysia. Also, schists, phyllite, slate as well as limestone are significant features of the lithology of Cameron Highlands [23]. The highlands are usually cloud-covered all year. The tropical forest, tea plantations and flower farms are the major land cover in the study area [36].

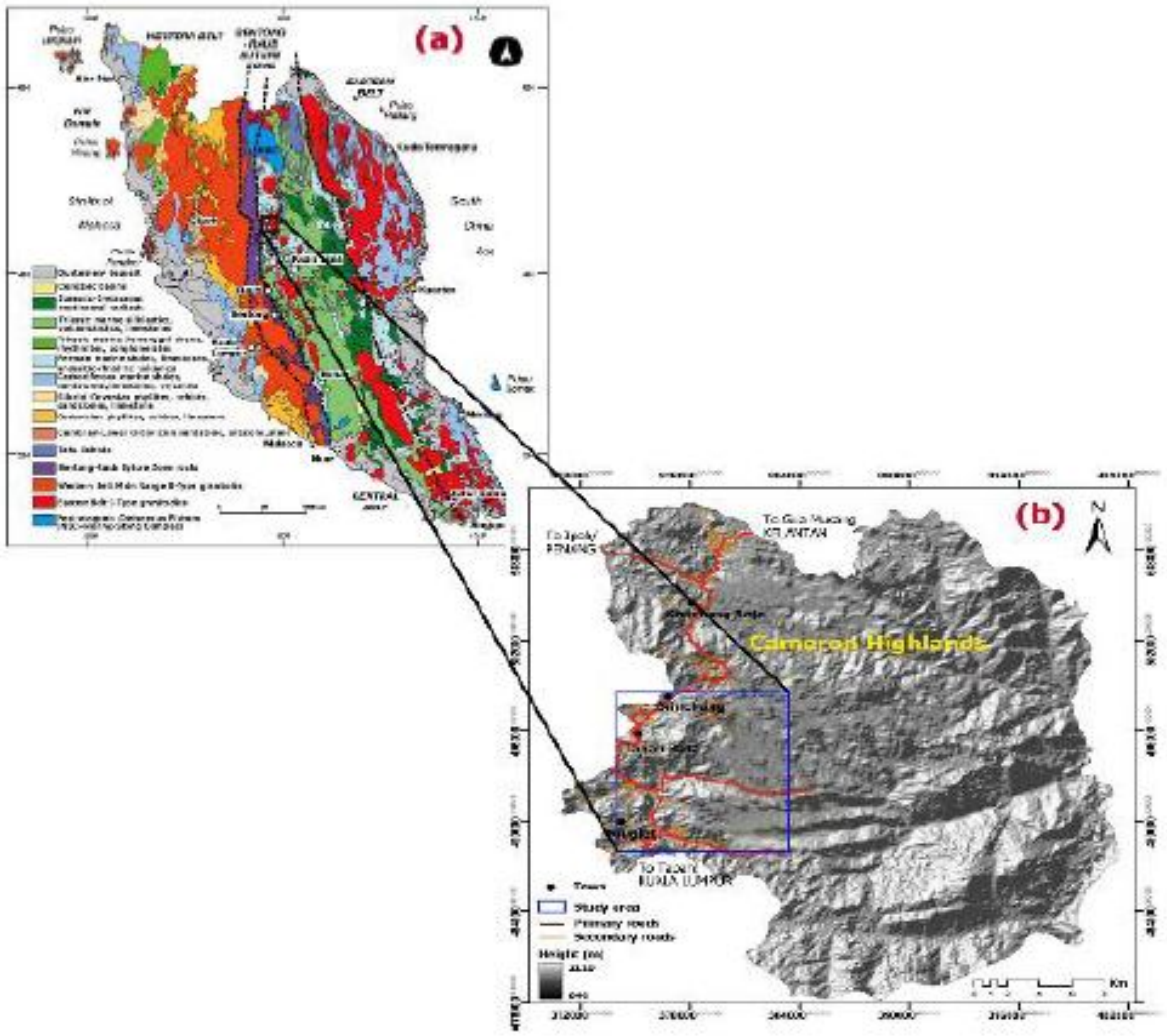


Fig. 1 Location of the study area in the Cameron Highlands, Peninsular Malaysia; (a) Simplified geological map of the peninsular Malaysia that modified from Metcalfe [23], (b) The district of the Cameron Highlands shown with a shaded relief map derived from a 30 m ASTER GDEM that modified from Razak [38]. The rectangular area represents the actual study area.

III. MATERIALS AND METHODES

Landslides mapping is difficult in tropical mountainous environments as dense vegetation growth obscures landslides soon after they occur [38]. Utilizing remote-sensing data such as optical satellite images and aerial photography interpretation are primary methods to obtain important, cost-effective information of landslide location [28]. The landslide information taken from remotely sensed images is especially associated with morphology, plant life, and hydrologic conditions of the region [29]. Several types of remote sensing data may be used in detecting landslide features, for instance, stereo-remote sensing products which in turn reveal the actual morphodynamical features of landslides [39]. In this study, published reports, field surveys, interpretation of digital aerial photographs (DAP) (10,000–1:50,000 scale) over a 25-year period, WorldView-1 satellite imagery on the March 2011, AIRSAR data on November 2004 has been utilized for extraction of

landslide inventory map. These black and white digital images with resolution=0.54 m pixel were taken during 1981–2006 and were acquired from the Malaysian Surveying and Mapping Department archives. In order to detect landslides which have occurred in the study area 6 digital aerial photographs were used requiring only one block of adjustment for the process and subsequently 4 stereo models were formed. WorldView-1 satellite data, which has a resolution of 0.46 meter for panchromatic band used to detect occurred landslides and to validate landslide inventory map was obtained from AIRSAR data in the study area. The AIRSAR data were collected over the study area on November 2004, during the PacRim1 campaign. AIRSAR flown in interferometric (TOPSAR) mode is capable of providing high resolution DEM datasets [30]. With a 40 MHz-10 km swath width and slant-range resolution 5x5 m, a DEM resolution of 10x10 m is achievable. The dataset used in this research consists of the DEM and C-, L- and P-band images. This dataset is to be compared with landslide features generated from aerial photographs and WorldView-1 satellite imagery which are also generated in UTM reference system. Multiple field investigations and ground control points (GCPs) were carried out by using global positioning system (GPS) to collect mapping information on landslide locations (See Fig. 2) and to generate stereo models from digital aerial photography data.



Fig. 2 Field photographs of recently occurred landslides and types of landslides;
(a) a shallow translational rockslide,
(b) a shallow translational debris slide at the road side,
(c) and (d) deep-seated rockslides. Arrow depicts the movement direction.

The DEM image was warped to the given ground control points in order to geo-reference the data. Then the image was further resized to the size equal to the size of sample area. At this stage the pixel resolution size was changed to a new resolution size of 2 m. All of the resultant sample area DEM heights were then used for height comparison with heights of DAP DEM and GPS GCPs in the assessment and correction processes. For the single C-band vv, the file was opened in ENVI 4.8 software was then converted to sigma zero (σ°) and finally to decibel (dBs).Later, this converted Cvv polarization data was combined with the L and P-band polarimetric data into a single file. Together they were then: masked, corrected from Antenna Pattern Correction (APC) and geo-referenced. The L and P bands files were opened in ENVI 4.8 software using the POLSAR Tools menu. The process was to decompress (synthesize) the Stoke Matrix files into six wavelength-polarization files that include: 1) L band; HH, HV and VV polarization, and 2) P band; HH, HV and VV polarization. After processing, the synthesized L and P-data were combined with the converted Cvv data into a new single file [49].

To identify landslides in the study area, three techniques were employed. The first technique was to compare directly by overlaying landslide vector images onto the DEMs and AIRSAR raster images. The second technique was to classify the images using ENVI 4.8 software. This is to separate landslides from the other land cover types in the surrounding area. The last technique is to separate landslides from the other land cover types in the surrounding area using segmentation followed by classification. This technique was carried out using software called “eCognition”. In eCognition software pixels are segmented into image object, so the image classification process in this software is image object based rather than pixel based classification that was previously carried out in ENVI 4.8 software [6].

The data used in segmentation were 1) C-, L- and P-band (wavelengths) with seven polarizations (Chh, Lhh, Lvv, Lhv, Phh, Pvv and Phv) images and 2) Slope image. In segmentation the information about the group of pixels inside the boundaries of landslide was used. The information include: 1) Spectral values of the C-, L- and P-band and 2) Average slope of the area.

Pixels inside the boundaries of landslide in each band image will have different spectral values [26]. These spectral values may represent spectral signatures of landslides. In segmentation processes using eCognition software, all three bands with seven polarizations and a slope image were combined to identify landslides in the images. If one existing landslide can be identified it can be used in the segmented image as a sample polygon. Using classification techniques, all other polygons that have the same characteristic of pixels brightness and average slope will be highlighted as similar [5].

Furthermore, the efficiency and quality of the SAR data and optical satellite images should be examined

using a proper method. The root mean square error (RMSE) method was used for accuracy of the obtained result [9, 3]. For each ground control points, the efficiency of the SAR data and optical satellite images is calculated based on the formula [9]:

$$RMSE = \sqrt{u^2 + v^2} \quad (1)$$

where u is residual in the x axis; v is residual in the y axis.

Total RMSE is then derived as (Eq.2):

$$TotalRMSE = \sqrt{\frac{1}{n}\sum_{i=1}^{n} u^2 + v^2} \quad (2)$$

where n is number of GCPs; u is residual in the x axis; v is residual in the y axis.

The total RMSE was calculated for each area, SAR and satellite optical image based on nearest neighbour resampling method [44].

IV. RESULTS AND DISCUSSION

The size and locations of landslides on the old landslide maps in the study area are inaccurate, therefore not suitable for any application in the landslide inventory map. Also, identified landslide is too small. Therefore the information about the pixel values might be insufficient for identifying landslide by segmentation and classification technique. Landslides can be identified on AIRSAR intensity image. The spectral values of the pixels representing landslides can be differentiated from the spectral values of the surrounding. Figure 3 shows the old landslide map overlaid onto the AIRSAR composite image. The composite image is one example among several composite images produced. In general because of the low resolution (10 m) and rough topography, it is difficult to differentiate the various land cover types. From the figure, the pixels within the boundaries of the landslides of the old landslide map could not be differentiated from the pixels outside the boundaries. Other tests using composite images and single images also gave similar results. Field observation was then carried out to check the existence and locations of the landslides shown in the old landslide map (See Fig. 3)

It was found that the landslides were difficult to locate and identify on the ground. In most cases the landslides have no trace. The scars are hidden by new undergrowth or are too small to be differentiated from surrounding features. Time difference between the production of the map (2004) and the field observation (2013) could be another reason. Heavy precipitation might also have wiped out the evidence of the landslides.

The procedures of composite images used in segmentation and classification is shown in Fig. 4. The procedures of composite images used in segmentation and classification include; a) the processed AIRSAR C-, L- and P-band image up to the image corrected with APC; b) the segmented image; c) the sampled image. The suspected landslides areas are in purple. The rest are other land cover types; d) the classification of the segmented image.

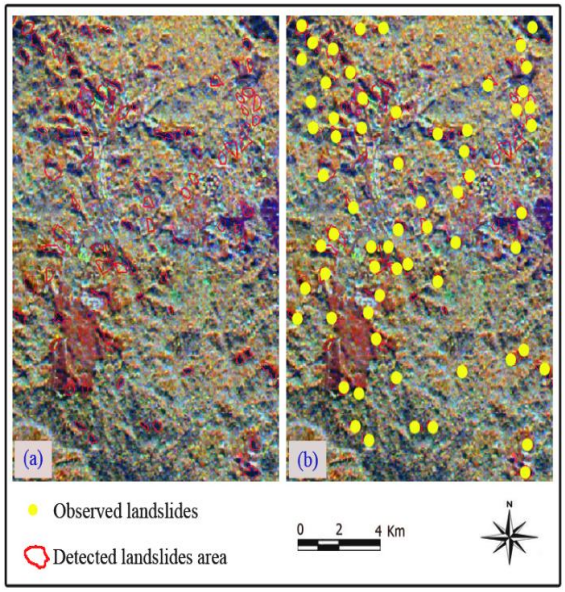


Fig. 3 The AIRSAR composite image is overlaid on the old landslides map; (a) Detected landslides, (b) Comparing detected and observed landslides.

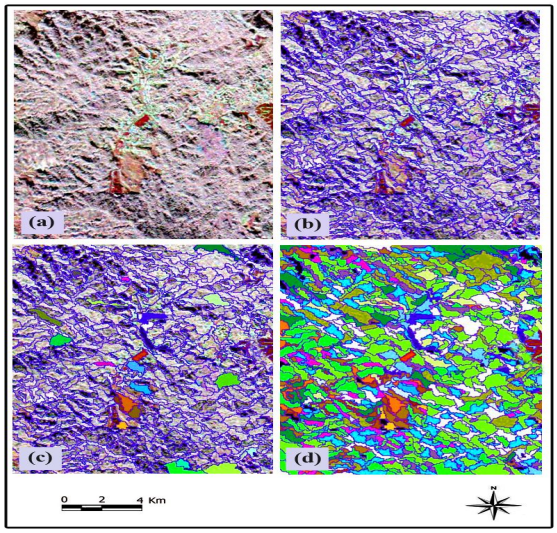


Fig. 4 The images of procedures for segmentation and classification on the AIRSAR images; (a) Cvv,Lhh,Lvv composite image, (b) Segmented with polygons, (c) Sampled, (d) Classified.

A classified section of the segmented image was overlaid on the old landslide map that shown in Fig. 5. The image shows that the landslide features of the old landslide map do not match the polygons classified as landslides. This indicates either the old landslide map is not accurate or the segmented areas of the AIRSAR C-, L- and P-band sampled as landslides are actually not a correct representation of the landslides because of incorrect positioning. Understandably if wrong segments were chosen and sampled as landslide areas,

the wrong pixel values will be used in the classification. Therefore wrongly classified landslides areas will be produced from the classification procedures. Nevertheless, as mentioned before the segments were chosen based on its closeness to the identified landsides on the old landslide map. Furthermore, the size and shape of the two segments are also similar to the corresponding landslide features of the old landslide map. They are also the closest segments to the rough positions of known landslides.

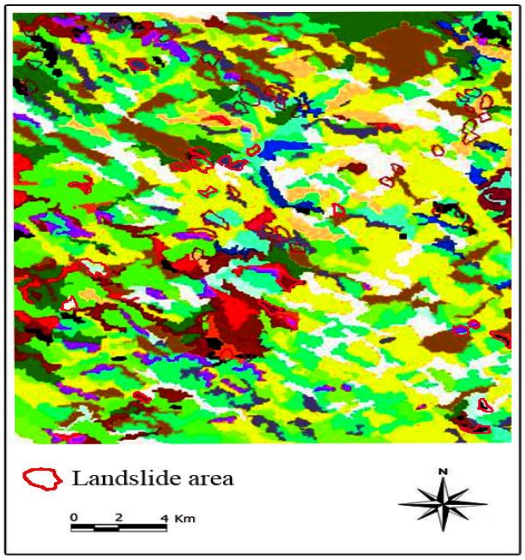


Fig. 5 The segmented and classified AIRSAR images overlaid with the old landslide map (landslides in red polygons).

Because of many problems with the old landslide map, validation of the map was the only way to check the accuracy. The landslides that were identified on the ground as mentioned previously were also identified on aerial photograph. To validate the landslide inventory map, the landslide features that were obtained from WorldView-1 satellite images were overlaid onto the C-, L- and P-band image. Since the landslide feature was in UTM reference system, C-, L- and P-band image in the UTM reference system was used.

The final landslide inventory map that was compiled in the present study is shown in Fig. 6. The results also identified that most of the landslides detected from AIRSAR data, digital aerial photographs and WorldView-1 satellite images are shallow rotational, and there are a few translational and flow types. In the present study, only the rotational landslides are counted, because the occurrences of the other types of landslides were scarce and very small. To assess the correctness and quality of the result, root mean square errors (RMSE) (Eqs. 1 and 2) was performed by comparing the in-situ measurements with the resulted one. The resulted RMSE was 0.163 which is acceptable and shows the efficiency of the proposed method in recognizing the landslides with high precision. The comparison between Figures 3 and 6 confirm that the landslide of the old landslide map is inaccurate in position and exaggerated in size.

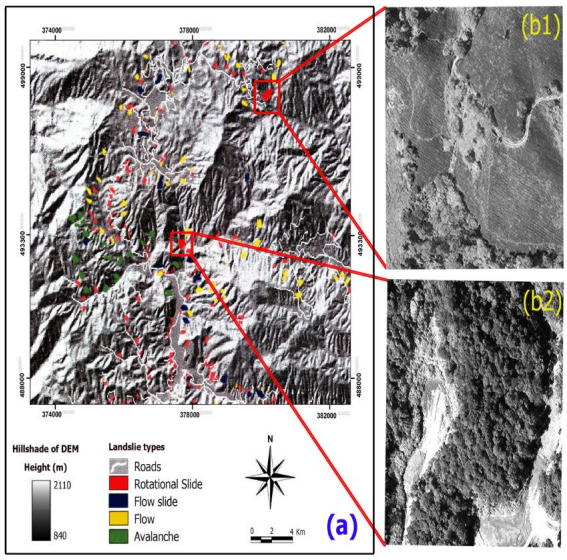


Fig.6 Final landslide inventory map extracted from AIRSAR data and WorldView-1 satellite images; (a) types of landslide locations overlaid on AIRSAR DEM, (b) enlarged views of two landslides locations on WorldView-1 satellite images (panchromatic band).

CONCLUSION

The research area because of its heavy rainfall and mountainous location has a typical landslide problem. In this study, landslides occurred frequently following precipitation. This is because the lithological and topography conditions are very appropriate for the creation of landslides. The research involved three main phases including landslide inventory analysis, susceptibility mapping and validation.

The landslide inventory map with a total of 92 landslide locations revealed the strong capability of AIRSAR data and WorldView-1 images satellite images to distinguish and detect the very small landslides of the earth surface which occurred due to the heavy precipitation with resulted accuracy of 0.163 RMSE. This RMCE accuracy is acceptable and shows the efficiency of the proposed method in recognizing landslides with high precision. Furthermore, current research revealed that the C-, L- and P-band image of AIRSAR data is able to provide acceptable coherence over highly vegetated areas.

Also, the integration of AIRSAR data with high resolution satellite images can play important role in the production of a landslide inventory map in tropical regions. The information provided by this landslide susceptibility map could be the basis for decision making, as planners and engineers can reduce losses caused by existing and future landslides by means of prevention, mitigation and avoidance.

REFERENCES

[1] Abella, E.C. and C. Van Westen, 2007.Generation of a landslide risk index map for Cuba using spatial multi-criteria evaluation. Landslides. 4(4): p. 311-325.

[2] Akgün, A. and F. Bulut, 2007.GIS-based landslide susceptibility for Arsin-Yomra (Trabzon, North Turkey) region. Environmental Geology. 51(8): p. 1377-1387.

[3] Askne, J. and M. Santoro, 2005.Multitemporal repeat pass SAR interferometry of boreal forests. Geoscience and Remote Sensing, IEEE Transactions on. 43(6): p. 1219-1228.

[4] Ayalew, L., H. Yamagishi, and N. Ugawa, 2004.Landslide susceptibility mapping using GIS-based weighted linear combination, the case in Tsugawa area of Agano River, Niigata Prefecture, Japan. Landslides. 1(1): p. 73-81.

[5] Blaschke, T. 2003. Object-based contextual image classification built on image segmentation. in Advances in Techniques for Analysis of Remotely Sensed Data, 2003 IEEE Workshop on. IEEE.

[6] Blaschke, T., 2010.Object based image analysis for remote sensing. ISPRS journal of photogrammetry and remote sensing. 65(1): p. 2-16.

[7] Corsini, A., et al., 2006.Space-borne and ground-based SAR interferometry as tools for landslide hazard management in civil protection. International Journal of Remote Sensing. 27(12): p. 2351-2369.

[8] Dai, F., C. Lee, and Y.Y. Ngai, 2002.Landslide risk assessment and management: an overview. Engineering geology. 64(1): p. 65-87.

[9] [9] Gibson, P.J., et al., 2000. Introductory remote sensing: digital image processing and applications. Vol. 11. Routledge London, UK.

[10] Günther, A., et al., 2014.Climate-physiographically differentiated Pan-European landslide susceptibility assessment using spatial multi-criteria evaluation and transnational landslide information. Geomorphology. 224: p. 69-85.

[11] Hizbaron, D.R., et al. 2011. Assessing social vulnerability to seismic hazard through spatial multi criteria evaluation in Bantul District, Indonesia. in Conference of Development on the Margin, Tropentag.

[12] ITC, I., ILWIS 3.0 academic user's guide. 2001. Enschede: ITC, Enschede, the Netherlands. 530.

[13] Joyce, K.E., et al., 2009.A review of the status of satellite remote sensing and image processing techniques for mapping natural hazards and disasters. Progress in Physical Geography.

[14] K. Ouchi, K., 2013.Recent trend and advance of synthetic aperture radar with selected topics. Remote Sensing. 5(2): p. 716-807.

[15] Kawabata, D. and J. Bandibas, 2009.Landslide susceptibility mapping using geological data, a DEM from ASTER images and an Artificial Neural Network (ANN). Geomorphology. 113(1): p. 97-109.

[16] Kayastha, P., M. Dhital, and F. De Smedt, 2013.Application of the analytical hierarchy process (AHP) for landslide susceptibility mapping: A case study from the Tinau watershed, west Nepal. Computers & Geosciences. 52: p. 398-408.

[17] Kouli, M., et al., 2010.Landslide hazard zonation in high risk areas of Rethymno Prefecture, Crete Island, Greece. Natural hazards. 52(3): p. 599-621.

[18] Kouli, M., et al., 2014.Landslide susceptibility mapping by comparing the WLC and WofE multi-criteria methods in the West Crete Island, Greece. Environmental Earth Sciences: p. 1-23.

[19] Komac, M., 2006.A landslide susceptibility model using the Analytical Hierarchy Process method and multivariate statistics in perialpine Slovenia. Geomorphology. 74(1): p. 17-28.

[20] Malczewski, J., 1999. GIS and multicriteria decision analysis. New York: Wiley

[21] Malczewski, J., 2004.GIS-based land-use suitability analysis: a critical overview. Progress in planning. 62(1): p. 3-65.

[22] Matori, A.N., A. Basith, and I.S.H. Harahap, 2012.Study of regional monsoonal effects on landslide hazard zonation in Cameron Highlands, Malaysia. Arabian Journal of Geosciences. 5(5): p. 1069-1084.

[23] Metcalfe, I., 2013.Tectonic evolution of the Malay Peninsula. Journal of Asian Earth Sciences. 76: p. 195-213

[24] Mondal, S. and R. Maiti, 2012.Landslide susceptibility analysis of Shiv-Khola watershed, Darjiling: a remote sensing & GIS based Analytical Hierarchy Process (AHP). Journal of the Indian Society of Remote Sensing. 40(3): p. 483-496.

[25] Nafooti, M.H. and M. Chabok Boldaje. 2011. Spatial prioritizing of pastures using spatial multi criteriaevaluation (Case study: Yoosef Abad watershed—Iran). in 2011 2nd International Conference on Environmental Engineering and Applications IPCBEE.

[26] Nichol, J. and M. Wong, 2005.Satellite remote sensing for detailed landslide inventories using change detection and image fusion. International Journal of Remote Sensing. 26(9): p. 1913-1926.

[27] Oh, H.-J. and B. Pradhan, 2011.Application of a neuro-fuzzy model to landslide-susceptibility mapping for shallow landslides in a tropical hilly area. Computers & Geosciences. 37(9): p. 1264-1276.

[28] Oh, H.-J., et al., 2012.Extraction of landslide-related factors from ASTER imagery and its application to landslide susceptibility mapping. International Journal of Remote Sensing. 33(10): p. 3211-3231.

[29] Qiao, G., et al., 2013.Landslide investigation with remote sensing and sensor network: From susceptibility mapping and scaled-down simulation towards in situ sensor network design. Remote Sensing. 5(9): p. 4319-4346.

[30] Panda, S.K., et al., 2010.Remote sensing and field-based mapping of permafrost distribution along the Alaska Highway corridor, interior Alaska. Permafrost and Periglacial Processes. 21(3): p. 271-281.

[31] Pohl, C. and J. van Genderen, 2014.Remote sensing image fusion: an update in the context of Digital Earth. International Journal of Digital Earth. 7(2): p. 158-172.

[32] Pourghasemi, H.R., M. Mohammady, and B. Pradhan, 2012.Landslide susceptibility mapping using index of entropy and conditional probability models in GIS: Safarood Basin, Iran. Catena. 97: p. 71-84.

[33] Pourghasemi, H., et al., 2014.GIS-based landslide susceptibility mapping with probabilistic likelihood ratio and spatial multi-criteria evaluation models (North of Tehran, Iran). Arabian Journal of Geosciences. 7(5): p. 1857-1878.

[34] Pradhan, B., 2010.Landslide susceptibility mapping of a catchment area using frequency ratio, fuzzy logic and multivariate logistic regression approaches. Journal of the Indian Society of Remote Sensing. 38(2): p. 301-320.

[35] Pradhan, B. and S. Lee, 2010.Regional landslide susceptibility analysis using back-propagation neural network model at Cameron Highland, Malaysia. Landslides. 7(1): p. 13-30.

[36] Pradhan, B., S. Lee, and M.F. Buchroithner, 2010.A GIS-based back-propagation neural network model and its cross-application and validation for landslide susceptibility analyses. Computers, Environment and Urban Systems. 34(3): p. 216-235.

[37] Rahman, R. and S. Saha, 2008.Remote sensing, spatial multi criteria evaluation (SMCE) and analytical hierarchy process (AHP) in optimal cropping pattern planning for a flood prone area. Journal of Spatial Science. 53(2): p. 161-177.

[38] Razak, K.A., et al., 2013.Generating an optimal DTM from airborne laser scanning data for landslide mapping in a tropical forest environment. Geomorphology. 190: p. 112-125.

[39] Roessner, S., et al., 2005.Potential of satellite remote sensing and GIS for landslide hazard assessment in Southern Kyrgyzstan (Central Asia). Natural Hazards. 35(3): p. 395-416.

[40] Saaty, T.L., 1977.A scaling method for priorities in hierarchical structures. Journal of mathematical psychology. 15(3): p. 234-281.

[41] Saaty, T.L., The analytic hierarchy process, 1980, New York: McGraw-Hill New York. p. 45-49.

[42] Sahnoun, H., et al., 2012.GIS and multi-criteria analysis to select potential sites of agro-industrial complex. Environmental Earth Sciences: p. 1-13.

[43] Shahabi, H., et al., 2014.Landslide susceptibility mapping at central Zab basin, Iran: A comparison between analytical hierarchy process, frequency ratio and logistic regression models. Catena. 115: p. 55-70..

[44] Shahabi, H., et al., 2014.Application of moderate resolution imaging spectroradiometer snow cover maps in modeling snowmelt runoff process in the central Zab basin, Iran. Journal of Applied Remote Sensing. 8(1): p. 084699-084699.

★★★